

# RSC Advances



This is an *Accepted Manuscript*, which has been through the Royal Society of Chemistry peer review process and has been accepted for publication.

*Accepted Manuscripts* are published online shortly after acceptance, before technical editing, formatting and proof reading. Using this free service, authors can make their results available to the community, in citable form, before we publish the edited article. This *Accepted Manuscript* will be replaced by the edited, formatted and paginated article as soon as this is available.

You can find more information about *Accepted Manuscripts* in the [Information for Authors](#).

Please note that technical editing may introduce minor changes to the text and/or graphics, which may alter content. The journal's standard [Terms & Conditions](#) and the [Ethical guidelines](#) still apply. In no event shall the Royal Society of Chemistry be held responsible for any errors or omissions in this *Accepted Manuscript* or any consequences arising from the use of any information it contains.



## Mechanistic outlook on thermal degradation of 1,3-dialkyl imidazolium ionic liquids and organoclays

Eapen Thomas, Deepthi Thomas, Kunduchi Periya Vijayalakshmi\* and Benny Kattikkal George

Received 00th January 20xx,  
Accepted 00th January 20xx

DOI: 10.1039/x0xx00000x

www.rsc.org/

The thermal degradation mechanisms of ionic liquids (ILs) 1-butyl-3-methylimidazolium chloride (BMImCl) and 1-butyl-3-methylimidazolium tetrafluoroborate (BMImBF<sub>4</sub>) have been established using pyrolysis-GC-MS (Py-GC-MS) and B3LYP/6-311+G(d,p) level of density functional theory (DFT). BMImCl decompose through a bimolecular nucleophilic substitution (S<sub>N</sub>2) while BMImBF<sub>4</sub> exhibit S<sub>N</sub>2 along with a competitive E2 elimination pathway. Activation energy parameters obtained using Kissinger-Akahira-Sunose method and Ozawa-Flynn-Wall method is compared with the computed activation barriers. The montmorillonite based organoclay prepared using these ionic liquids absorbs only the cation part ([BMIm]<sup>+</sup>) into the clay gallery leading to an expansion of d-spacing from 12.08 to 13.64 Å. The organoclay showed the maximum decomposition at 462 °C in the TGA experiment and the decomposition products were identified as methyl imidazole and 1-butene using Py-GC-MS. DFT studies employing a model compound Si(OH)<sub>3</sub>O<sup>-</sup> suggested a mechanism involving an imidazole-2-ylidene (carbene) intermediate for the decomposition of [BMIm]<sup>+</sup> in the clay. Theoretical results were further supported by <sup>13</sup>C NMR analysis of IL in presence of colloidal silica which showed a characteristic carbene NMR signal at 187.6 ppm.

### 1. Introduction

Ionic liquids (ILs) are a class of novel compounds typically composed of organic cations and inorganic or organic anions. ILs have large liquid ranges determined by their low melting point and high decomposition temperature. The high thermal stability of ILs attracted intense research interest owing to their applications in various fields such as energetic materials,<sup>1,2</sup> solvents for organic reactions,<sup>3</sup> solvents for cellulose,<sup>4</sup> thermal energy storage,<sup>5</sup> clay modifiers to form thermally stable polymer composites,<sup>6</sup> heat-transfer fluids,<sup>7</sup> high-temperature lubricants,<sup>8</sup> curing of ionogels<sup>9</sup> and as a stationary phase in gas chromatography.<sup>10</sup> It is well known that the physical and chemical properties of ILs vary with the choice of anion and cation while thermal stability is often tuned by the choice of anions.

For safe application of ILs at elevated temperatures, it is important to understand the degradation mechanism. The nucleophilic attack of the halide at primary alkyl substituents in imidazolium ring is known to be the major degradation pathway in N,N-dialkyl imidazolium halides.<sup>11-16</sup> Chowdhury *et al*<sup>17</sup> showed that imidazolium based ILs decompose at lower temperatures in the presence of nucleophiles. Baranyai *et al*<sup>18</sup> investigated the thermal decomposition mechanism of 1,3-dialkyl imidazolium bis(trifluoromethylsulfonyl) imide ILs, and suggested degradation of the anion as possible thermal decomposition pathway, but the anion degradation products were not detected. Lazzus<sup>19</sup> introduced a group contribution method and Yan *et al*<sup>20</sup> used quantitative structure property relationship method to predict the thermal decomposition temperature of ILs. Ohtani *et al*<sup>21</sup> studied decomposition of imidazolium ILs using Py-GC-MS and proposed mechanism based on the products formed. Quantum mechanical

tools have also been extensively used to understand the degradation mechanism of compounds.<sup>22-26</sup>

In spite of the several reports on the thermal stability of ILs,<sup>27-30</sup> systematic studies correlating the structural features as well as the degradation mechanism to understand the thermal stability of ILs are scarce. In the present study, the degradation reactions of 1-butyl-3-methylimidazolium chloride (BMImCl), 1-butyl-3-methylimidazolium tetrafluoroborate (BMImBF<sub>4</sub>) and 1-butyl-3-methylimidazolium modified montmorillonite clay (Clay-BMIm) are analyzed using Py-GC-MS and formation of pyrolysis products are rationalized using density functional theory (DFT). We have proposed a new mechanism for decomposition of 1,3-dialkylimidazolium modified clays in general by taking into consideration of Clay-BMIm. To the best of our knowledge, this is the first report on thermal decomposition mechanism of 1,3-dialkylimidazolium incorporated montmorillonite clay.

### 2. Methodology

#### 2.1 Materials

BMImCl and BMImBF<sub>4</sub> of purity >99% were procured from M/s Otto Chemie Pvt. Ltd, Mumbai, India. Clay used was Sodium montmorillonite (trade name: Cloisite-Na<sup>+</sup>, CAS no. 1318-93-0, Southern Clay Products, Inc., USA) for the ion exchange modification with ILs. Colloidal silica (30% suspension of SiO<sub>2</sub> in water, CAS No. 7631-86-9) was obtained from Sigma Aldrich.

#### 2.2 Functionalization of clay

Standard ion exchange procedures were employed for the functionalization of sodium montmorillonite clay (MMT) with ILs.<sup>31</sup> Aqueous suspension of MMT clay (2 %) was prepared by sonicating for 10 minutes using Hielscher-UIP1000hd probe sonicator at amplitude of 80 %. To this, BMImCl (or BMImBF<sub>4</sub>, both yield same product Clay-BMIm) was added and the exchange reactions were

Analytical and Spectroscopy Division, Analytical, Spectroscopy and Ceramics Group, Propellants, Polymers, Chemicals and Materials Entity, Vikram Sarabhai Space Centre, Thiruvananthapuram- 695022, India  
E-mail: vijisura@gmail.com, kp\_vijayalakshmi@vssc.gov.in

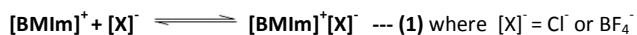
carried out by sonicating for 15 minutes. It was allowed to settle and filtered. The residue was repeatedly (5-8 times) washed with distilled water until no chloride traces were detected with silver nitrate solution. The residue (modified MMTs) was dried at room temperature for 4 h and then at 100 °C for 2 hour under vacuum. Characterisation of modified clay is included in the supporting information (ESI).

### 2.3 Instrumental

Thermal stability of ILs and Clay-BMIIm were studied using Perkin Elmer, Pyris-1 TGA (Shelton, USA) in He atmosphere at a heating rate of 10 °C/min. Py-GC-MS studies were carried out using a system consists of a Thermo Electron Trace ultra GC directly coupled to a Thermo Electron PolarisQ (Quadrupole ion trap) mass spectrometer (Thermo Electron Corporation, Waltham, Massachusetts, USA) and SGE pyrolyser (Pyrojector II, SGE Analytical Science Pty Ltd, Ringwood, Victoria, Australia). The GC is equipped with 30 m, 0.25 mm ID capillary column (PDMS with 5 % phenyl, SLB-5MS, Supelco). The Py-GC-MS conditions were set with ion source at 200 °C, inlet at 250 °C, transfer line at 280 °C, column temperature programme 40 °C to 250 °C with heating rate of 10 °C/min. The m/z range used was 20-600 amu and the pyrolysis was carried out at 350 °C and 600 °C. <sup>13</sup>C NMR analysis using Bruker Avance-III 400 MHz spectrometer operated at 100.2 MHz with power 54 W, pulse width 8.9 μs and D<sub>2</sub>O as locking solvent.

### 2.4 Computational method

Geometries of gaseous ion pairs of BMIImCl, BMIImBF<sub>4</sub>, transition states and products were optimized at B3LYP<sup>32</sup> level of DFT using 6-311+G(d,p) basis set as implemented in *Gaussian09*.<sup>33</sup> All the transition states were confirmed by the presence of single imaginary frequency. The single step conversion is further analysed using IRC calculations (ESI). Molecular electrostatic potential (MESP) derived Merz-Singh-Kollman charge (MK charge)<sup>34,35</sup> was computed at the same level of theory. Basis set superposition error corrected binding energy<sup>36</sup> for the ion-pairs ([BMIIm]<sup>+</sup>[X]<sup>-</sup>) was calculated using eqn. (1).



### 2.5 Kinetic studies

Kinetic parameters for the thermal decomposition of ILs were calculated using two methods, Kissinger-Akahira-Sunose (KAS) method<sup>37-39</sup> and Ozawa-Flynn-Wall (FWO) method.<sup>40-42</sup> KAS is a multiple heating rate method and we have selected heating rate of 2, 5, 10 and 15 °C/min. KAS method is based on the following eqn. 2

$$\ln \frac{\beta}{T_\alpha^2} = \ln \left[ \frac{AR}{g(\alpha)E_a} \right] - \frac{E_a}{RT_\alpha} \quad \text{--- (2)}$$

Where  $\beta$  is the heating rate,  $T_\alpha$  is the temperature in Kelvin corresponding to a fixed degree of conversion  $\alpha$ , A is the pre-exponential factor, R is the gas constant,  $E_a$  is the activation energy at a given degree of conversion and  $g(\alpha)$  is the integral form of kinetic model function.  $E_a$  for a given degree of conversion is obtained from the slope of the linear fit of the plot  $\ln \frac{\beta}{T_\alpha^2}$  versus  $1/T_\alpha$ . FWO method for determination of kinetic parameters is based on the assumption that the decomposition obeys first order kinetics using a point of constant conversion from a series of decomposition curves obtained at different heating rates. It helps in calculating the  $E_a$  for a desired conversion (Eqn.3).

$$E_a = \left( \frac{R}{b} \right) * \left( \frac{\Delta \log[\beta]}{\Delta (1/T)} \right) \quad \text{--- (3)}$$

Where  $b = 0.457$  initially and it depends on the value of  $E/RT$ .<sup>39</sup> value of  $b = 0.471, 0.453$  and  $0.456$  respectively for BMIImCl, BMIImBF<sub>4</sub> and Clay-BMIIm (ESI).

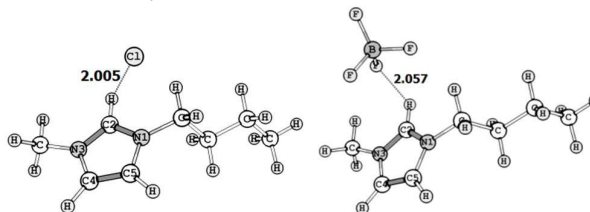


Fig. 1. Optimized structures of BMIImCl and BMIImBF<sub>4</sub> at B3LYP level of DFT.

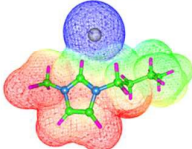
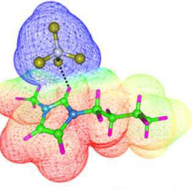
## 3. Results and Discussion

### 3.1 Electronic structure and properties of ion pairs

Optimized structures of BMIImCl and BMIImBF<sub>4</sub> at B3LYP/6-311+G(d,p) level of DFT are shown in Fig. 1. In BMIImCl, the distances of the C2H...Cl (2.005 Å) are much longer than the covalent bond distance of H-Cl (1.31 Å) and shorter than the van der Waals distance of H...Cl (2.95 Å). Similarly in BMIImBF<sub>4</sub>, the shortest distance of C2H...F between the imidazolium cation and the anion (2.057 Å) are higher than covalent bond distance of H-F (1.07 Å) and smaller than the van der Waals distance of H-F (2.67 Å). The non-covalent binding energy ( $E_b$ ) computed for ILs are very high, 373.4 kJ/mol and 340.2 kJ/mol respectively for BMIImCl and BMIImBF<sub>4</sub>, indicating strong electrostatic interactions in ion pairs. The geometric features as well as the  $E_b$  values of these ion pairs agreed very well with those reported by Dong *et al*.<sup>43</sup> and Fumino *et al* at B3LYP/6-31+G(d) level.<sup>44</sup> The MK charge can be considered as a measure of charge transfer from the anion to the cation. Higher charge transfer was observed for BMIImCl (23 %) than BMIImBF<sub>4</sub> (12 %) (Table 1).

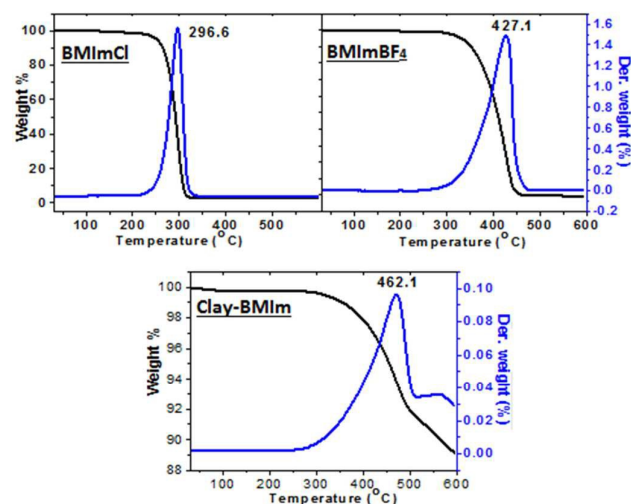
Generally the stability of a salt system is assessed by the large energy gap between the highest occupied molecular orbital and the lowest unoccupied molecular orbital (HOMO-LUMO gap).<sup>45</sup> Since, the charge transfer is more conducive in BMIImCl than BMIImBF<sub>4</sub>, the latter with higher HOMO-LUMO gap (6.88 eV) can be considered as a more stable salt than BMIImCl, which can be further supported by TG analysis.

Table 1. MESP plots, MESP-derived charges,  $E_b$  and HOMO-LUMO gap of ion pairs.

| IL                   | MESP plot & MK charge (a.u)  | $E_b$ (kJ/mol) | HOMO-LUMO gap (eV) |
|----------------------|--|----------------|--------------------|
| BMIImCl              | <br>Charge(anion):-0.768 | -373.4         | 4.08               |
| BMIImBF <sub>4</sub> | <br>Charge(anion):-0.882 | -340.2         | 6.88               |

### 3.2. TG analysis

Fig. 2 shows the TG curves for BMImCl, BMImBF<sub>4</sub> and Clay-BMIm. The higher initial decomposition temperature observed for BMImBF<sub>4</sub> (260 °C) compared to BMImCl (180 °C), suggests the role of counter anion on thermal stability of ILs. The maximum decomposition temperatures (T<sub>s</sub>) are 297, 427 and 462 °C respectively for BMImCl, BMImBF<sub>4</sub> and Clay-BMIm. The differences in the decomposition of selected ILs with different anions and Clay-BMIm, without an anion suggests the possibility of different mechanisms for their thermal decomposition reactions. In Clay-BMIm the weight loss observed between 500 °C and 600 °C was attributed to the dehydroxylation of structural hydroxyl groups.<sup>46</sup>



**Fig. 2.** TG curves for BMImCl, BMImBF<sub>4</sub> and Clay-BMIm in He atmosphere at a heating rate of 10 °C/min.

$E_a$  for thermal decomposition of BMImCl, BMImBF<sub>4</sub> and Clay-BMIm were calculated using KAS method and FWO method (Table 2). The calculated  $E_a$  values showed 6 % deviation for BMImCl, 8 % for BMImBF<sub>4</sub> and 9 % for Clay-BMIm (ESI).

**Table 2.** Kinetic studies using TG.

| $\beta$ (°C/min)    | KAS method          |     |     |     | $E_a$ (kJ/mol) | FWO method<br>$E_a$ (kJ/mol) |
|---------------------|---------------------|-----|-----|-----|----------------|------------------------------|
|                     | T <sub>s</sub> (°C) |     |     |     |                |                              |
|                     | 2                   | 5   | 10  | 15  |                |                              |
| BMImCl              | 257                 | 285 | 297 | 300 | 101.5          | 107.4                        |
| BMImBF <sub>4</sub> | 402                 | 411 | 427 | 432 | 236.8          | 258.0                        |
| Clay-BMIm           | 437                 | 442 | 462 | 468 | 229.3          | 208.5                        |

### 3.3 Decomposition mechanism

#### 3.3.1 BMImCl

Fig. 3 shows the pyrogram of BMImCl at two different temperatures, 350 and 600 °C. Four major decomposition products were identified, 1-chloromethane ( $m/z = 50$ ), 1-chlorobutane ( $m/z = 92$ ), 1-methylimidazole ( $m/z = 82$ ) and 1-butylimidazole ( $m/z = 124$ ). A decomposition mechanism based on the products obtained on pyrolysis is shown in Scheme 1.

The dealkylation reaction is initiated by the nucleophilic attack of chloride anion at the alkyl group of imidazolium cation which passes through the bimolecular nucleophilic (S<sub>N</sub>2) transition state. Kroon et al<sup>22</sup> used B3LYP at 6-31G\*\* level to predict the

decomposition products of BMImCl. For pathway-I,  $E_a$  was 127 kJ/mol while for pathway-II, a higher value 136 kJ/mol was observed.

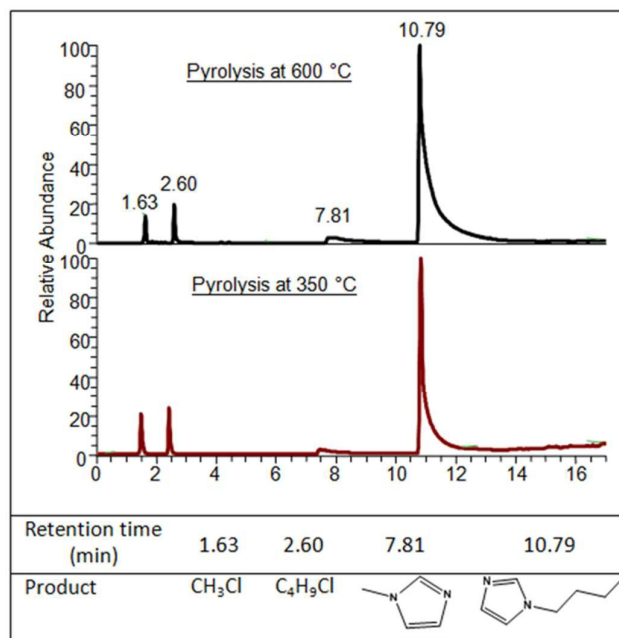
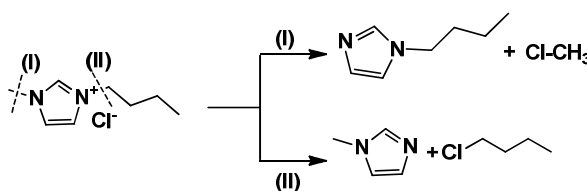


**Fig. 3.** Pyrogram and decomposition products of BMImCl at 350 and 600 °C.

Semi quantitative estimation using standard solutions of 1-butylimidazole and 1-methylimidazole shows that 90 % of the products are from pathway-1 (ESI). We have calculated  $E_a$  of reaction pathways shown in scheme 1 at a higher level, B3LYP/6-311+G(d,p) to confirm the product distribution as calculated from Py-GC-MS. Transition states identified and energy profile are shown in Fig. 4.



**Scheme 1.** Decomposition route of BMImCl.

Demethylation reaction (pathway-I) proceed with an  $E_a$  of 122.7 kJ/mol while debutylation reaction proceed with an  $E_a$  of 130.8 kJ/mol (Fig. 4). These results match with Kroon et al<sup>22</sup> and shows the selectivity for pathway-I even though the  $E_a$  differ only by 8 kJ/mol and the higher percentage of butylimidazole is accounted. Consequently the net  $E_a$  for the reaction was 123.5 kJ/mol (Table 3) and experimental values for  $E_a$  were 101.5 kJ/mol and 107.4 kJ/mol calculated using KAS and FWO methods respectively. The results showed a deviation of 13 % with FWO method and 18 % with KAS method (Table 3). DFT studies also predict that both demethylation and debutylation reactions of BMImCl are endothermic with ~10 kJ/mol and DSC analysis shows endotherm for the same (ESI).

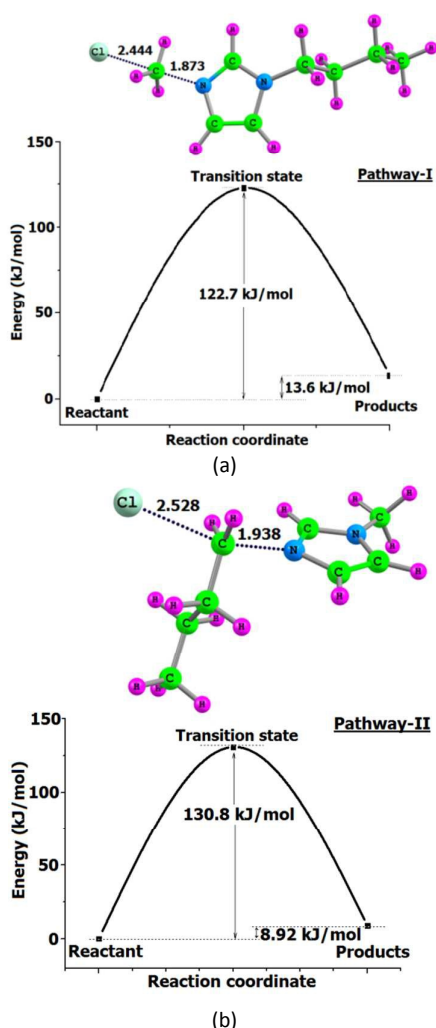


Fig. 4 Energy profile and transition states of BMImCl decomposition shown in Scheme 1. (a) Pathway-I and (b) Pathway-II. Bond lengths in Å.

### 3.3.2 BMImBF<sub>4</sub>

Pyrogram of BMImBF<sub>4</sub> at 600 °C is shown in Figure 5. Major peaks in the pyrogram are identified as 1-butene ( $m/z = 56$ ), 1-methylimidazole ( $m/z = 82$ ) and 1-butylimidazole ( $m/z = 124$ ).

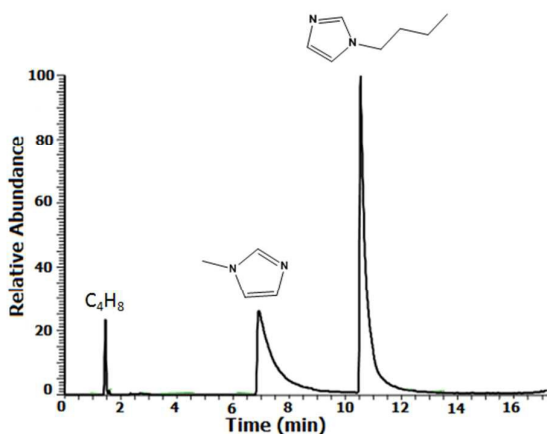
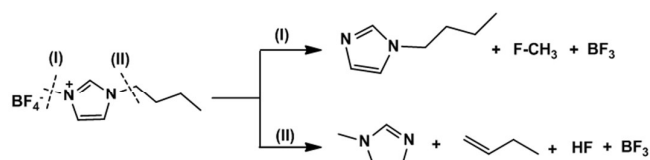


Fig. 5 Pyrogram of BMImBF<sub>4</sub> at 600 °C.

Owing to the steric bulkiness of BF<sub>4</sub><sup>-</sup> compared to Cl<sup>-</sup>, the S<sub>N</sub>2 reactions are likely to happen only at the N3-CH<sub>3</sub> site (Scheme-2) and it is unambiguous with the presence of butyl imidazole as the major product in the pyrogram.



Scheme 2. Decomposition routes of BMImBF<sub>4</sub>

Differing from BMImCl, the presence of 1-butene in the pyrogram suggests existence of competitive elimination reactions in the thermal decomposition of BMImBF<sub>4</sub>. Three different elimination mechanism namely bimolecular E2 elimination, internal elimination and elimination via imidazol-2-ylidene (carbene route)<sup>47,48</sup> were analyzed by DFT (ESI) and transition state was identified only for E2 elimination (pathway-II).

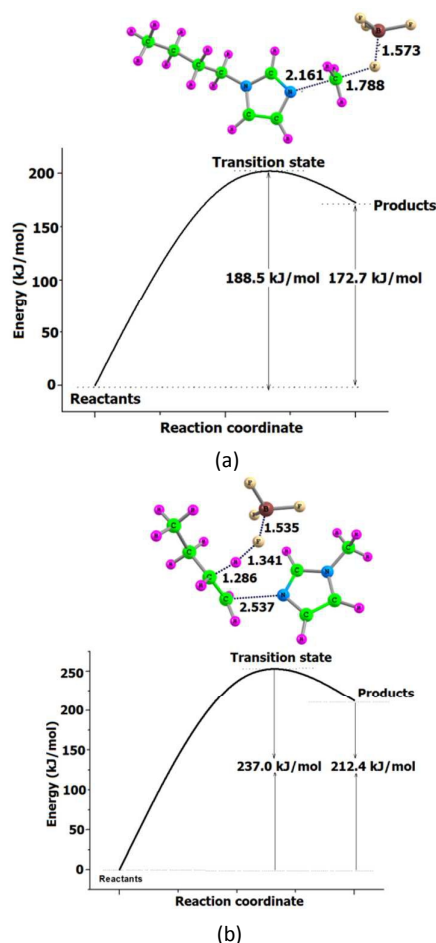


Fig. 6. Energy profile for (a) pathway-I (S<sub>N</sub>2 mechanism) and (b) pathway-II (E2 Elimination). Transition states are also shown with distance parameters in Å.

Though the intramolecular elimination reactions (Ei) are common in pyrolysis reactions, in the case of BMImBF<sub>4</sub> the basicity of the anion overrules and E2 elimination is found to be preferred over Ei route, as the basicity of BF<sub>4</sub><sup>-</sup> anion is insufficient to form the imidazol-2-

ylidene which is expected to undergo further abstraction of  $\beta$ -hydrogen to form the pyrolysis products viz. butene and methyl imidazole (ESI).

Computed activation barrier for the formation of butyl imidazole, (Fig. 6) is 188.5 kJ/mol (195 kJ/mol by Kroon et al.<sup>22</sup> at B3LYP/6-31\*\* level of DFT) and is higher than the corresponding value for BMImCl (122.7 kJ/mol, Fig.4, Pathway-I). Transition state for E2 elimination was characterized by a four membered ring with breaking of C-N bond at C...N distance 2.537 Å and simultaneous  $\beta$ -hydrogen shift. The activation barrier for this reaction was 237 kJ/mol (Fig.6). The experimental values depicted in Table 2 using KAS method (236.8 kJ/mol), FWO method (258.0 kJ/mol) and a higher concentration of 1-butene and 1-methylimidazole in the pyrogram suggest the possibility of interplay of both the mechanisms in decomposition of BMImBF<sub>4</sub>. The ratio of 1-methylimidazole to 1-butylimidazole was determined by a semi quantitative method as in the case of BMImCl and observed both reactions proceed equally (1:1) (ESI). The average  $E_a$  predicted using DFT was 212.1 kJ/mol (Table 3) and the deviation between computed and experimental  $E_a$  may be due to the lattice energy change in experiments where ILS in liquid phase are analysed unlike gas phase calculations in computational method. Both the mechanisms discussed are highly endothermic (172-212 kJ/mol) as shown in Fig.6 and confirmed using DSC analysis (ESI).

Table 3. Comparison of computed and Experimental  $E_a$  with extend of reaction (% Rn) for BMImCl and BMImBF<sub>4</sub>.

|                     | Computational Study |            |                      |            | Experimental      |                  |                   |                  |      |
|---------------------|---------------------|------------|----------------------|------------|-------------------|------------------|-------------------|------------------|------|
|                     | SN <sub>2</sub> (I) |            | SN <sub>2</sub> (II) |            | KAS Method        |                  | FWO Method        |                  |      |
|                     | $E_a$<br>(kJ/mol)   | Rn.<br>(%) | $E_a$<br>(kJ/mol)    | Rn.<br>(%) | $E_a$<br>(kJ/mol) | Deviation<br>(%) | $E_a$<br>(kJ/mol) | Deviation<br>(%) |      |
| BMImCl              | 122.7               | 90         | 130.8                | 10         | 123.5             | 101.5            | 17.8              | 107.4            | 13.0 |
| BMImBF <sub>4</sub> | E <sub>2</sub>      |            |                      |            |                   |                  |                   |                  |      |
|                     | 188.5               | 51         | 237.0                | 49         | 212.1             | 236.8            | 10.4              | 258.0            | 17.8 |

### 3.3.3 Clay-BMIm

In the present study organoclays were prepared using BMImCl and characterized (ESI). Thermal stability of Clay-BMIm was studied using TGA (Fig.2) and decomposition products were identified as butene and methyl imidazole using Py-GC-MS (Fig. 7)

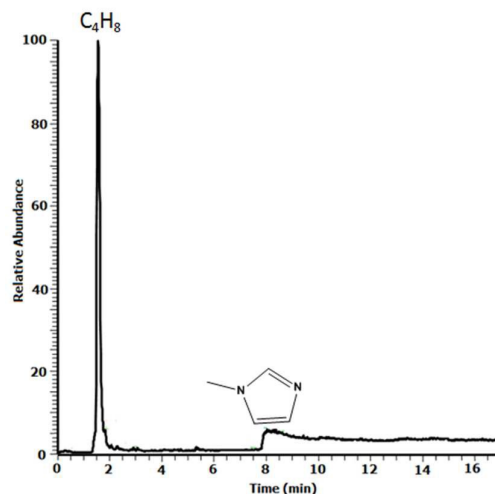


Fig. 7 Pyrogram of Clay-BMIm at 600 °C.

Thermal decomposition of Clay-BMIm was analysed using DFT method. MMT clays own a pyrophyllite structure where the trivalent Al-cation in the octahedral layer is partially substituted by

the divalent Mg-cation. Consequent negative charge generated in the clay layer is balanced by hydrated sodium ions adsorbed in the interlayer. The interlayer dimension is determined by the crystal structure of the silicate and the d-spacing is  $\sim$ 1 nm for MMT clay. From the model of MMT clay given in Fig. 8, it is clear that the ions in the interlayer gallery face SiO<sub>4</sub> tetrahedral unit as their immediate neighbour.<sup>49</sup> In Clay-BMIm sodium ions are replaced by 1-butyl-3-methylimidazolium cation.

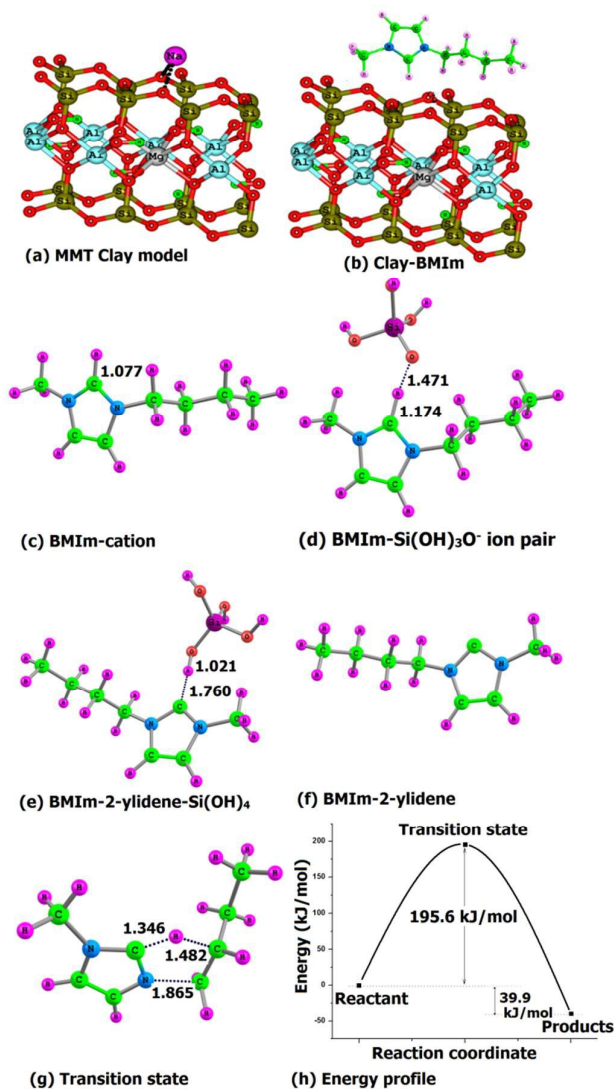
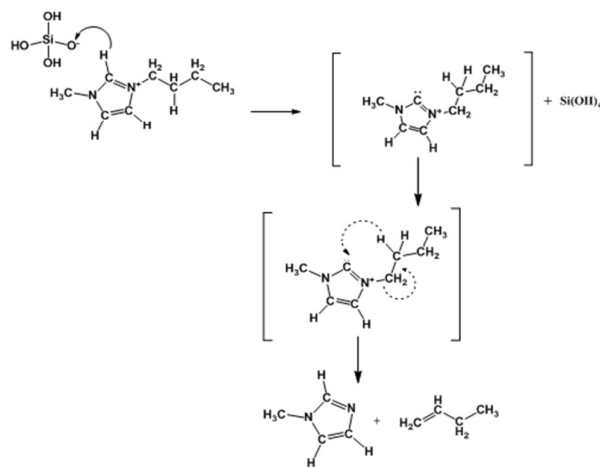


Fig. 8. (a) Model structure of MMT clay, (b) Clay-BMIm, (c - h) Optimized structures of species involved in decomposition of Clay-BMIm with transition state and energy profile.

A truncated model for the montmorillonite clay showing the interaction of Na<sup>+</sup> with oxygen atoms that bridges two silicon centers is presented in Fig. 8a. The [BMIm]<sup>+</sup> could replace the Na<sup>+</sup> cation owing to extended interaction of several CH bonds on to the layer dominated by Si-O bonds. Considering the negatively charged character of the clay and the possible CH<sup>+</sup>O-Si interactions from [BMIm]<sup>+</sup> to the clay, we propose the use of the anionic moiety Si(OH)<sub>3</sub>O<sup>-</sup> to model the decomposition reaction of [BMIm]<sup>+</sup> in the clay.



**Fig. 9.** Mechanism of Clay-BMIIm decomposition through 1-butyl-3-methylimidazol-2-ylidene route.

BMIIm-Si(OH)<sub>3</sub>O<sup>-</sup> ion pair is found to be marginally higher in energy (9.1 kJ/mol) than the neutral complex of imidazole-2-ylidene-Si(OH)<sub>4</sub> (Fig. 8). Therefore the DFT results suggest that the intercalated imidazolium cations can easily form the imidazol-2-ylidene through a barrier less pathway. The singlet carbenes thus formed on heating can undergo elimination reactions involving beta hydrogen shift from the butyl substituent at N1 to the carbenic centre followed by bond breaking at the quaternary nitrogen. Such a transition state was located in the DFT analysis with single imaginary frequency corresponding to the bond shifting process which is shown in Fig. 8(g).

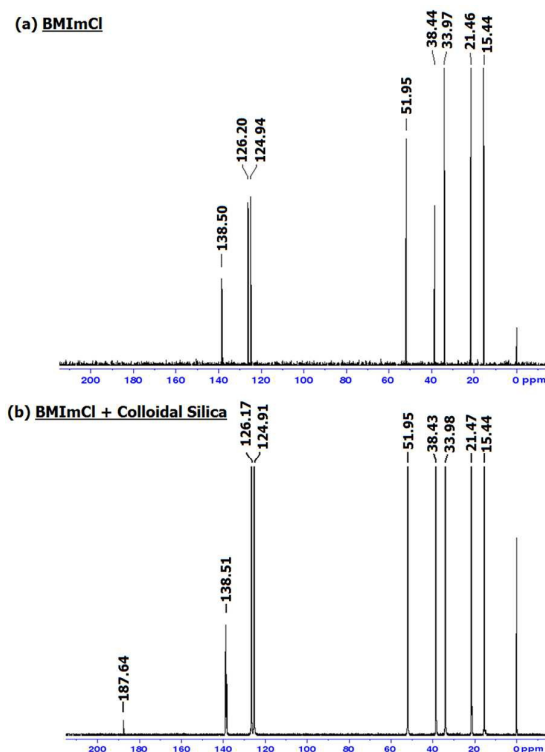


**Fig. 10.** <sup>13</sup>C NMR spectrum of (a) BMIImCl in D<sub>2</sub>O and (b) BMIImCl with colloidal silica in D<sub>2</sub>O after heating.

The activation energy for the decomposition was 195.6 kJ/mol (Fig. 8(h) and the reaction is exothermic by 39.9 kJ/mol and DSC analysis shows an exotherm for the same (ESI). The summarized decomposition mechanism is shown in Fig. 9. Anions with high basicity is capable of deprotonating imidazolium cation at C2 position, resulting in the formation of neutral carbon bases with nucleophilic singlet carbenes that are stabilized by the two neighboring nitrogen atoms at the carbenic centre. The formation of carbene from BMIIm cation on heating was confirmed by the NMR analysis of BMIImCl in D<sub>2</sub>O solvent in presence of colloidal silica. Colloidal silica is 30 % suspension of SiO<sub>2</sub> in water, which contains -SiOH species similar to our model compound Si(OH)<sub>3</sub>O<sup>-</sup> used in DFT study. <sup>13</sup>C NMR spectra of BMIImCl and BMIImCl with colloidal silica heated at 90 °C for 5 minutes are shown in Fig. 10. The additional NMR signal observed at 187.64 ppm is attributed to singlet carbene carbon in imidazolium ring.

#### 4. Conclusions

Thermal stability of BMIImCl and BMIImBF<sub>4</sub> were compared using TGA and decomposition products were identified using Py-GC-MS experiments. The inherent stability of BMIImBF<sub>4</sub> is attributed to their very high HOMO-LUMO gap as well as the higher MK charge computed for ion-pair counterparts. Bimolecular nucleophilic substitution reactions are identified to be the lowest energy pathway for decomposition of both the ions pairs. However, BF<sub>4</sub><sup>-</sup> anion facilitates competitive E2 elimination reactions in imidazolium based ILs. The extend of reactions were calculated from Py-GC-MS and DFT results. Demethylation reaction of BMIImCl constitutes 90 % of the reaction. Decomposition of BMIImBF<sub>4</sub> proceeds with 50 % demethylation and 50 % elimination reaction. For the first time the thermal degradation of ionic liquid modified clay was elucidated using DFT and experimentally rationalized using Py-GC-MS and <sup>13</sup>C-NMR experiments.

#### 5. Acknowledgement

The authors thank Director, Vikram Sarabhai Space centre for granting permission to publish this work. One of the authors (ET) thanks Indian Space Research Organization for providing research fellowship. The authors also thank Dr. Suresh C. H., CSIR-National Institute for Interdisciplinary Science and Technology, Trivandrum for the revision and valuable comments.

#### Abbreviations

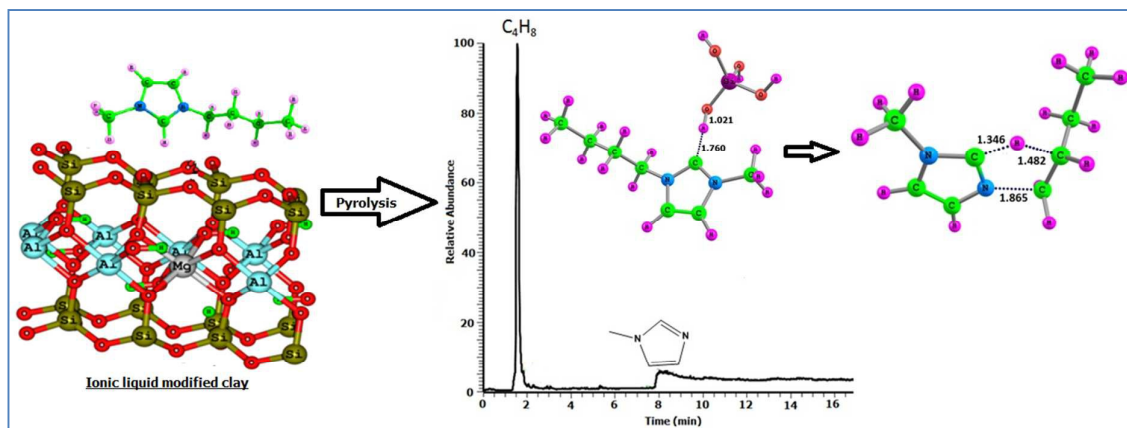
|                                 |   |
|---------------------------------|---|
| IL                              | ionic liquid                                  |
| [BMIIm] <sup>+</sup>            | 1-butyl-3-methylimidazolium cation            |
| BMIImCl                         | 1-butyl-3-methylimidazolium chloride          |
| BMIImBF <sub>4</sub>            | 1-butyl-3-methylimidazolium tetrafluoroborate |
| MMT                             | Montmorillonite clay                          |
| Clay-BMIIm                      | Clay modified with ILs                        |
| DFT                             | density functional theory                     |
| [BF <sub>4</sub> ] <sup>-</sup> | tetrafluoroborate anion                       |
| E <sub>a</sub>                  | activation energy                             |
| E <sub>b</sub>                  | binding energy                                |
| T <sub>s</sub>                  | maximum decomposition temperature             |
| HOMO                            | highest occupied molecular orbital            |
| LUMO                            | lowest unoccupied molecular orbital           |
| ΔE <sup>*</sup>                 | energy gap between the HOMO and LUMO          |
| MK charge                       | Merz-Singh-Kollman charge                     |
| KAS                             | Kissinger-Akahira-Sunose method               |
| FWO                             | Osawa-Flynn-Wall method                       |

## References

1. E. Sebastiao, C. Cook, A. Hu and M. Murugesu, *J. Mater. Chem. A*, 2014, **2**, 8153-8173.
2. E. Thomas, K. P. Vijayalakshmi and B. K. George, *RSC advances*, 2015, **5**, 71896-71902.
3. R. H. Wang, C. M. Jin, B. Twamley and J. M. Shreeve, *Inorg. Chem.*, 2006, **45**, 6396-6403.
4. F. Wendler, L. N. Todi and F. Meister, *Thermochim. Acta*, 2012, **528**, 76-84.
5. L. Bai, X. Li, J. Zhu and B. Chen, *Energy Fuels*, 2011, **25**, 1811-1816.
6. J. Gilman, W. H. Awad, R. D. Davis, J. Shields, R. H. Harris, C. Davis, A. B. Morgan, T. E. Sutto, J. Callahan, P. C. Trulove and H. C. DeLong, *Chem. Mater.*, 2002, **14**, 3776-3785.
7. E. B. Fox, A. E. Visser, N. J. Bridges and J. W. Amoroso, *Energy Fuels*, 2013, **27**, 3385-3393.
8. Z. Zeng, B. S. Phillips, J. C. Xiao and J. M. Shreeve, *Chem. Mater.*, 2008, **20**, 2719-2726.
9. J. L. Bideau, L. Viau and A. Vioux, *Chem. Soc. Rev.*, 2011, **40**, 907-925.
10. Z. Breitbach and D. Armstrong, *Anal. Bioanal. Chem.*, 2008, **390**, 1605-1617.
11. H. L. Ngo, K. LeCompte, L. Hargens and A. B. McEwen, *Thermochim. Acta*, 2000, **357-358**, 97-102.
12. T. Erdmenger, J. Vitz, F. Wiesbrock and U. S. Schubert, *J. Mater. Chem.*, 2008, **18**, 5267-5273.
13. A. G. Glenn and P. B. Jones, *Tetrahedron Letters*, 2004, **45**, 6967-6969.
14. L. Bai, X. Li, J. Zhu and B. Chen, *Energy Fuels*, 2011, **25**, 1811-1816.
15. C. Maton, N. D. Vos and C. V. Stevens, *Chem. Soc. Rev.*, 2013, **42**, 5963-5977.
16. K. R. J. Lovelock, J. P. Armstrong, P. Licence and R. G. Jones, *J. Phys. Chem. Chem. Phys.*, 2014, **16**, 1339-1353.
17. A. Chowdhury and S. T. Thynell, *Thermochim. Acta*, 2006, **443**, 159-172.
18. K. J. Baranyai, G. B. Deacon, D. R. MacFarlane, J. M. Pringle and J. L. Scott, *Aust. J. Chem.*, 2004, **57**, 145-147.
19. J. A. Lazzús, *Journal of Molecular Liquids*, 2012, **168**, 87-93.
20. F. Yan, S. Xia, Q. Wang and P. Ma, *J. Chem. Eng. Data*, 2012, **57**, 805-810.
21. H. Ohtani, S. Ishimura and M. Kumai, *Anal. Sci.*, 2008, **24**, 1335-1340.
22. M. C. Kroon, W. Buijs, C. J. Peters and G. J. Witkamp, *Thermochim. Acta*, 2007, **465**, 40-47.
23. S. Reshmi, K. P. Vijayalakshmi, D. Thomas, B. K. George and C. P. Reghunadhan Nair, *J. Anal. Appl. Pyrolysis*, **2013**, **104**, 603-608.
24. Z. Xue, Y. Zhang, X. Zhou, Y. Cao and T. Mu, *Thermochimica Acta*, 2014, **578**, 59-67.
25. P. Ballone and R. C. Huerto, *Faraday Discuss.*, 2012, **154**, 373-389.
26. Y. Hao, J. Peng, S. Hu, J. Li and M. Zhai, *Thermochimica Acta*, 2010, **501**, 78-83.
27. Y. Cao and T. Mu, *Ind. Eng. Chem. Res.*, 2014, **53** (20), 8651-8664.
28. W. H. Awad, J. W. Gilman, M. Nyden, R. H. Harris, T. E. Sutto, J. Callahan, P. C. Trulove, H. C. DeLong and D. M. Fox, *Thermochim. Acta*, 2004, **409**, 3-11.
29. C. P. Fredlake, J. M. Crosthwaite, D. G. Hert, S. N. V. K. Aki and J. F. Brennecke, *J. Chemical & Engineering Data*, 2004, **49**, 954-964.
30. M. E. Van Valkenburg, R. L. Vaughn, M. Williams and J. S. Wilkes, *Thermochim. Acta*, 2005, **425**, 181-188.
31. L. B. de Paiva, A. R. Morales and F. R. V. Diaz, *J. Applied Clay Science*, 2008, **42**, 8-24.
32. A. D. Becke, *Phys. Rev. A*, 1988, **38**, 3098-3100.
33. Gaussian 09, Revision A.1, M. J. Frisch, G. W. Trucks, H. B. Schlegel, G. E. Scuseria, M. A. Robb, J. R. Cheeseman, G. Scalmani, V. Barone, B. Mennucci, G. A. Petersson, H. Nakatsuji, M. Caricato, X. Li, H. P. Hratchian, A. F. Izmaylov, J. Bloino, G. Zheng, J. L. Sonnenberg, M. Hada, M. Ehara, K. Toyota, R. Fukuda, J. Hasegawa, M. Ishida, T. Nakajima, Y. Honda, O. Kitao, H. Nakai, T. Vreven, J. A. Montgomery, Jr., J. E. Peralta, F. Ogliaro, M. Bearpark, J. J. Heyd, E. Brothers, K. N. Kudin, V. N. Staroverov, R. Kobayashi, J. Normand, K. Raghavachari, A. Rendell, J. C. Burant, S. S. Iyengar, J. Tomasi, M. Cossi, N. Rega, J. M. Millam, M. Klene, J. E. Knox, J. B. Cross, V. Bakken, C. Adamo, J. Jaramillo, R. Gomperts, R. E. Stratmann, O. Yazyev, A. J. Austin, R. Cammi, C. Pomelli, J. W. Ochterski, R. L. Martin, K. Morokuma, V. G. Zakrzewski, G. A. Voth, P. Salvador, J. J. Dannenberg, S. Dapprich, A. D. Daniels, O. Farkas, J. B. Foresman, J. V. Ortiz, J. Cioslowski, D. J. Fox, Gaussian Inc., Wallingford CT, 2009.
34. U. C. Singh and P. A. Kollman, *J. Comp. Chem.*, 1984, **5**, 129-145.
35. B. H. Besler, K. M. Merz Jr. and P. A. Kollman, *J. Comp. Chem.*, 1990, **11**, 431-39.
36. S. F. Boys and F. Bernardi, *Mol. Phys.*, 1970, **19**, 553-566.
37. H. Tanaka, *Thermochimica Acta.*, 1995, **267**, 29-44.
38. S. Vyazovkin, K. Chrissafis, M. L. Di Lorenzo, N. Koga, M. Pijolat and B. Roduit, *Thermochimica Acta.*, 2014, **590**, 1-23.
39. B. V. L'Vov, *Spectrochimica Acta Part B: Atomic Spectroscopy*, 2011, **66** (7), 557-564.
40. ASTM, Standard Test Method for Decomposition Kinetics by Thermogravimetry, E-1641-1699.
41. T. Ozawa, *Bulletin of the Chemical Society of Japan*, 1965, **88**, 1881-1886.
42. J. H. Flynn and L. A. wall, *Polymer Letters*, 1966, **4**, 323-328.
43. K. Dong, S. Zhang, D. Wang and X. Yao, *J. Phys. Chem. A*, 2006, **110**, 9775-9782.
44. K. Fumino, A. Wulf and R. Ludwig, *Phys. Chem. Chem. Phys.*, 2009, **11**, 8790-8794.
45. G. Zhao and M. Lu, *J. Mol. Model.*, 2012, **16**, 2443-2451.
46. P. Singla, R. Mehta and S. N. Upadhyay, *Green and Sustainable Chemistry*, 2012, **2**, 21-25.
47. O. Holloczki, D. Gerhard, K. Massone, L. Szarvas, B. Nemeth, T. Veszpremi and L. Nyulaszi, *New J. Chem.*, 2010, **34**, 3004-3009.
48. E. A. Turner, C. C. Pye and R. D. Singer, *J. Phys. Chem. A*, 2003, **107**, 2277-2288.
49. S. Cadars, R. Guegan, M. N. Garaga, X. Bourrat, L. L. Forestier, F. Fayon, T. V. Huynh, T. Allier, Z. Nour and D. Massiot, *Chem. Mater.*, 2012, **24**, 4376-4389.



## Table of content graphics



Thermal decomposition of ionic liquid modified sodium montmorillonite clay proceed through an imidazol-2-ylidene (carbene) mediated mechanism with an activation energy of 195.6 kJ/mol.